HAL
open science

Electron-electron interactions in nano-patterned La 0.3 Sr 0.7 MnO 3 thin films

Laurie E Calvet, Guillaume Agnus, Philippe Lecoeur

To cite this version:

Laurie E Calvet, Guillaume Agnus, Philippe Lecoeur. Electron-electron interactions in nano-patterned La 0.3 Sr 0.7 MnO 3 thin films. Journal of Vacuum Science & Technology A, 2019, 37 (3), pp.031504. 10.1116/1.5085669 . hal-02389082

HAL Id: hal-02389082

https://hal.science/hal-02389082v1

Submitted on 2 Dec 2019

HAL is a multi-disciplinary open access archive for the deposit and dissemination of scientific research documents, whether they are published or not. The documents may come from teaching and research institutions in France or abroad, or from public or private research centers.

L'archive ouverte pluridisciplinaire **HAL**, est destinée au dépôt et à la diffusion de documents scientifiques de niveau recherche, publiés ou non, émanant des établissements d'enseignement et de recherche français ou étrangers, des laboratoires publics ou privés.

Electron-electron interactions in nano-patterned $La_{0.3}Sr_{0.7}MnO_3$ thin films

Laurie E. Calvet[a)], Guillaume Agnus, Philippe Lecoeur

Centre de Nanosciences et Nanotechnologies- CNRS UMR 9001, 10 Avenue Gobert, Université Paris-Sud, Université Paris-Saclay, Palaiseau, 91120 France,

[a)] Electronic mail: laurie.calvet@c2n.upsaclay.fr

Understanding the transport in ultra-thin epitaxial $La_{0.3}Sr_{0.7}MnO_3$ (LSMO) is a topic wide-spread current interest. Here we explore electron-electron interactions in low temperature magneto-transport in straight and zig-zag nanowires fabricated from ultra-thin epitaxial LSMO films grown to different thicknesses on STO(100) substrates. We find that three-dimensional electron-electron interactions can explain the resistivity upturn, including many of the changes observed with film thickness, nano-patterning, and magnetic field.

I. INTRODUCTION

At low temperatures quantum mechanical corrections to the resistivity of metals and doped semiconductors can lead to a minimum and a subsequent increase of the resistance. Such effects are often attributed to one or a combination of two mechanisms:[1]

weak localization (WL), due to the backscattering of phase coherent electrons interfering constructively, and/or electron-electron interactions (EEI), which occur when the screening of diffusive electrons is enhanced compared to the conventional Fermi liquid model. These phenomena have been broadly investigated in nonmagnetic materials of all dimensions[1,2]. They are typically disentangled by exploring magnetoresistance because changes from WL typically occur at very low magnetic fields (< 1 T), while changes from EEI will appear at much larger fields. Magnetic materials have been considered recently and a large amount of research has shown that the interplay between these quantum phenomena and the magnetism can be difficult to disentangle. [3–16]

In manganite materials the interplay between electronic, magnetic and structural degrees of freedom can further complicate the interpretation of the data. [17–27] Even at low temperatures the magnetoresistance due to the ferromagnetism can be larger than typical quantum corrections and can vary greatly both in materials with different constituents and in the same material with different thicknesses, growth parameters and substrates. Variations in the transport properties can also be attributed to changes in strain of the manganite[17]. In addition, in polycrystalline materials a resistivity minimum may also be due to antiferromagnetically aligned grains[18–20]. Previous reports concerning the resistivity minimum in magnetic oxides have shown that electron-electron interactions are by the far the most commonly observed phenomena[20–26], although weak localization has also been demonstrated[26–28], as well as anti-localization in very high purity films[29].

Here we investigate low temperature transport behavior in manganite devices patterned by electron beam lithography and ion beam etching. In the 50-300K temperature range, we have shown that the electronic transport of such devices are

electronically representative of the thin film behavior[30]. By examining structures with different thicknesses, nanofabrication patterning here we explore the dimensionality of the samples and the competition between electron-electron interactions and other effects.

II. EXPERIMENTAL DETAILS

Epitaxial LSMO thin films were deposited on (100) oriented $SrTiO_3$ (STO) substrates by pulsed laser deposition at 685°C and an O_2 pressure of 120 x 10^{-3} Torr. Film thicknesses of 9.6 ± 0.2 nm, 20.8 ± 0.4 nm and 27 ± 0.4 nm were determined from X-ray diffraction using reflectivity for the thinnest film and thickness fringes around the diffraction peak for the thicker two. Devices were patterned in a 3-step process via optical and electron beam lithography and ion beam etching, as described previously.[31] The different device characteristics are summarized in Table 1, and SEMs of two devices are shown in the insets of Fig. 1. SEMs for the other devices are included in Fig. S1 of the supplementary material at [URL will be inserted by AIP Publishing].

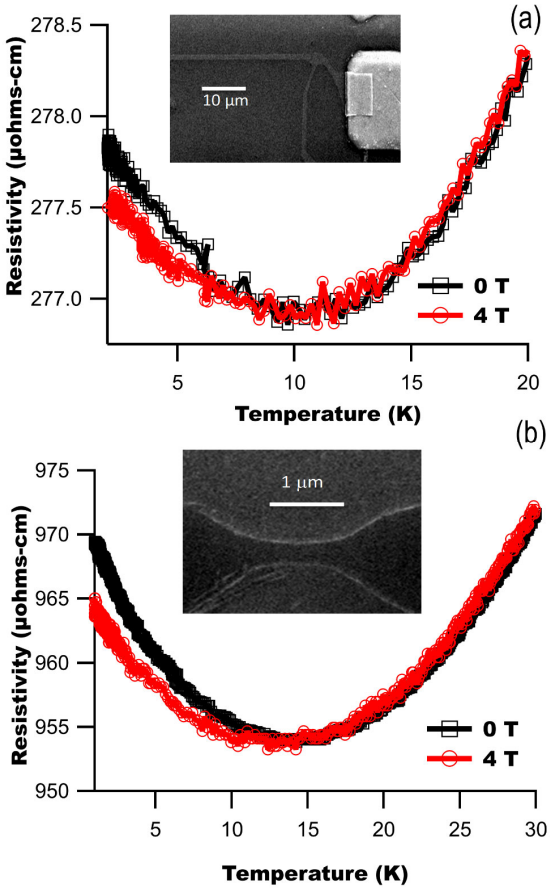

FIG. 1. (a) Resistivity versus temperature at 0 T and 4 T for a) PLD 608 dev 8 and b) PLD 683, dev 17. The curves are normalized so that the minimum of the 4 T curve overlaps that of the 0 T curve. The insets show SEMs of the devices. SEMs and curves for all devices are shown in Fig. S1 and Fig. S3 respectively.

TABLE I. Key characteristics of the different devices. The shape column indicates the geometry of the device. 'V' and 'W' indicate a V and W type nano-patterning, as shown in the supplementary material, in which the transport is along the (100) direction. 'NW' indicates a straight nanowire with the transport along the (110) easy axis. The 'W'

nanowires in PLD683 dev 22 had widths of 119 nm, comparable to the NW in PLD683 dev 6. Note that the magnetic field data for PLD608 dev 8 was done at 4 T.

Dev ref	t nm	l µm	w µm	Shape	ρ_{min} mΩ-cm	T_{min} (0T) K	upturn (0T) %	T_{min} (5T) K	upturn (5T) %
PLD664 dev 16	27 ± 0.4	2	0.13	V	0.231	10.3	0.3	10.4	0.21
PLD664 dev 30	27 ± 0.4	2	0.11	V	0.265	11.7	0.29	11.7	0.21
PLD608 dev 8	20.8 ± 0.4	30	0.8	NW	0.277	11.6	0.39	11.93	0.43
PLD608 dev 9	20.8 ± 0.4	30	0.35	NW	0.254	10.7	0.50	12.5	0.61
PLD683 dev17	9.6 ± 0.2	1.67	0.4	NW	0.955	14.3	1.7	12.2	1.1
PLD683 dev6	9.6 ± 0.2	1.8	0.138	NW	0.593	14.5	1.9	15.3	1.05
PLD683 dev22	9.6 ± 0.2	$\sum_i \frac{l_i}{w_i} = 42.3$		W	0.479	13.94	4	14.57	2.2

Four point measurements were first performed to verify that the contacts did not add a series resistance to the devices and tunnel junction behavior was not observed at any temperature. I-V measurements showing ohmic behavior are included in Fig. S2 of the supplementary material. More detailed two terminal measurements were performed in a split coil magnet with a cryostat insert with temperatures varied from 1-300 K. All magnetic fields in this paper were oriented perpendicular to the surface of the thin film. Standard lock-in techniques were used, with the AC voltage V_{ac} from the lock-in biased across a 100 kΩ or 1 MΩ resistor and a measurement of the voltage across the device. The AC current source could be varied between 250 nA and 1 mA. Other than Joule heating at large AC currents, the changes in the AC current source had no noticeable effect on the measurements. This measurement set-up allowed an extremely fine

resolution of ~0.01% of the resistivity minimum in order to determine the resistivity upturn shown in the results.

To obtain the % upturn, ρ_{min}, T_{min} in Table 1, we first fit the data at higher temperatures to a single magnon with a localized impurity band model[30,32] with form:

$$\rho = \rho_0 + bT^{2.5} \quad (1)$$

We then fit the data at lower temperatures to the three-dimensional electron-electron interactions, discussed in greater detail below, of form:

$$\rho = \rho_0 + K\sqrt{T} \quad (2)$$

where K is a constant. We find the intersection of these two curves, and denote it by ρ_{min} and T_{min} and take the % upturn from ρ_{min} and and ρ at T = 2 K. An example of this is given in Fig. 2. The fitting parameters and standard deviations are provided in Table S1 of the supplementary material.

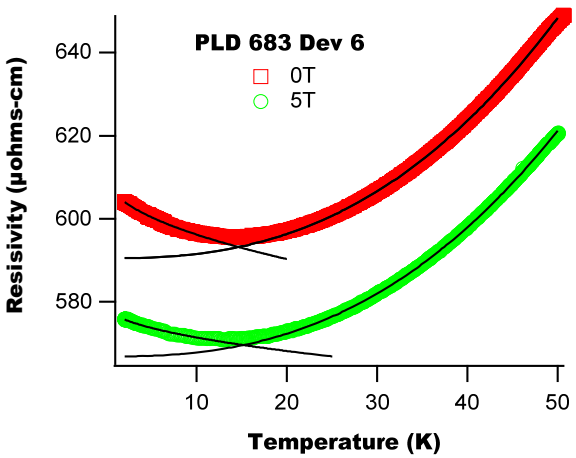

Fig. 2 Resistivity upturn at 0T and 5T for PLD 683 Device 6 showing the data (markers) and fits to Eqs (1) and (2) above where the intersection was used to determine % upturn, ρ_{min}, T_{min} for Table 1.

Note that we have not carried out measurements of straight nanowires in the (100) direction and thus cannot tell if differences in the magnitude of ρ_{min} in the zigzag versus

straight nanowires are due to patterning or to transport direction. Nevertheless they do permit us to understand some of the different aspects of nano-patterning on electro-electron interactions as discussed below.

III. MODELING

In conventional solid state theory electron-electron interactions are accounted for by Fermi liquid theory, where an electron is viewed as a quasiparticle with a screening cloud surrounding an electronic charge. In the late 1970s, Altshuler and Aronov showed that the disordered Fermi liquid could give rise to additional effects resulting in singularities that can become important at low temperatures[1]. They showed that in 3 dimensions (3D) corrections to the conductivity take the form:

$$\Delta\sigma = \frac{e^2}{4\hbar\pi^2}\frac{1.3}{\sqrt{2}}\left(\frac{4}{3} - \frac{3}{2}\widetilde{F_\sigma^{3D}}\right)\sqrt{\frac{k_B T}{2\hbar D}} \tag{3}$$

where Δσ is the change in conductance from its low temperature maximum, e is electronic charge, $\hbar$ is Planck's constant, k_B is Boltzmann's constant, T is temperature, and D is the diffusion coefficient. To connect eq (3) with eq (2), we note $\Delta\rho = \rho - \rho_0 = \rho_0^2\Delta\sigma$. The constant $\breve{F}_\sigma^{3D}$ is related to the relative contributions of the exchange (first term) and Hartree (second term) terms and is a measure of screening. It is given by:

$$\breve{F}_\sigma^{3D} = \frac{32}{3F}\left[\left(1 + \frac{1}{2}F\right)^{\frac{3}{2}} - 1 - \frac{3}{4}F\right] \tag{4}$$

where F can be approximated by:

$$F = \left(\frac{k_0}{2k_f}\right)^2 \ln(1 + \left(\left(\frac{2k_f}{k_0}\right)^2\right). \tag{5}$$

From the Thomas-Fermi screened potential we recall that $k_0 = \sqrt{\frac{eN(E_f)}{\varepsilon_0}}$ is the inverse screening length where $N(E_F)$ is the density of states, assumed to be ~ 2.4 x 10^{22} /eV/cm^3 [33], and ε_0 is the electric constant. In 2 dimensions (2D) the conductivity corrections are:

$$\Delta\sigma = \frac{e^2}{4\hbar\pi^2}\left(2 - \frac{3}{2}\check{F}_\sigma^{2D}\right) ln\left(\frac{T}{T_{min}}\right) \quad (6)$$

where

$$\check{F}_\sigma^{2D} = \frac{8}{F}\left(1 + \frac{1}{2}F\right)\ln\left(1 + \frac{1}{2}F\right) - 4. \quad (7)$$

$\check{F}_\sigma$ is a measure of screening, with values close to 0 implying low screening and close to one high screening. Note that T_{min} is the temperature corresponding to ρ_{min}.

A previous theoretical report of the screening factor found $\check{F}_\sigma^{3D}$= 0.46 was based on an estimation of k_f using the free electron approximation with periodic boundary conditions and an effective mass equal to the electron mass[26]; however, Angle Resolved Photoemission Spectroscopy ARPES measurements have shown that $k_f \approx 0.49\ \pi/a$ = 4.051 x 10^9/m where a = 3.8 Å, is the lattice constant of LSMO.[34] Others have theoretically reported $\check{F}_\sigma^{2D}$= 0.87 (ref 20), and a $k_f \approx$ = 7 x 10^{-9} /m (ref 30). Both $1/k_F$ and $1/k_0$ are smaller than any dimension in the device and thus we use only the 3D versions of these two parameters and obtain F = 0.93, corresponding to $\check{F}_\sigma^{3D}$= 0.87 and $\check{F}_\sigma^{2D}$= 0.81.

For electron-electron interactions, the dimensionality of the system is based on the thermal diffusion length, which is the electron-electron correlation length: $l_t = \left(\frac{\hbar D}{k_B T}\right)^{\frac{1}{2}}$ where D is the diffusion coefficient for the material, $\hbar$ is Planck's constant, k_B is Boltzman's constant and T is temperature. To calculate the diffusion coefficient from the conductivity, the Einstein relation for degenerate conductors ($D = {}^{1}/_{\rho_{min} e^2 n(E)}$) is used

where ρ_{min} is the resistivity minimum. Without ambiguity we use the 3D diffusion coefficient because the mean free path $l_e = v_f \tau_e$ (~ 0.6 nm) in this material is smaller than the thicknesses used here. A magnetic field will affect only the *Hartree* term and will *increase* the correction from electron-electron interactions. Nevertheless, the short scattering times found in metals renders the magnetoresistance from EEI (<< 0.01 % at 5 T) negligible here.

Weak localization results from the quantum interference associated with the enhanced probability that an electron's trajectory will return to its initial position. In 3D the conductivity correction due is given by a power law in temperature that depends on the dominant collision mechanism[1]. In 2D, it follows a natural logarithmic dependence. The system changes dimensionality when one of its dimensions becomes smaller than the phase coherence length: $L_\Phi = \sqrt{D\tau_\varphi}$. In traditional metals, weak localization is investigated as a function of small magnetic fields to obtain the electron dephasing time τ_ϕ and its temperature dependence. In magnetic materials, such experiments are difficult because the magnetic moment can change the resistivity and obscure WL. Typically, small magnetic fields have a large effect on quantum interference.

IV. RESULTS AND DISCUSSION

A. Results

Fig. 1 shows an example of the resistivity versus temperature in the <110> for two nano-patterned devices with different thicknesses and similar graphs of all devices are given in S3 of the supplementary material. The basic results for the 7 devices are summarized in Table 1. We can distinguish the devices by comparing the thickness, the

width and the shape of the nanowires. First, we note that ρ_{min} is on average slightly increased from for the 21 nm thickness versus the 27 nm devices but a significantly larger increase is observed in the 9.6 nm thick devices of PLD683. The general trend for larger ρ_{min} with decreasing thickness is also observed in the width dependence of the two devices in PLD664. However, it is the opposite from what is observed in the width dependence of the devices in PLD608 and PLD683, which exhibit *larger* ρ_{min} with *larger width*. Table S1 shows that ρ_{min} always decreases with field, a well-established effect in manganites.

$T_{\min}$ follows the same dependence as ρ_{min} for thickness in devices PLD608 and PLD 664. However, for PLD683 $T_{\min}$ is smaller for the wider device. In a magnetic field $T_{\min}$ does not exhibit a specific trend and is discussed in more detail in the section IV.B.

The resistivity upturn is what allows us to connect the results with the quantum corrections, either electron-electron or weak localization. The general trend for the thickness dependence is that the upturn is larger for larger ρ_{min}, however the dependence on nano-patterning is not as clear-cut. In PLD683 the largest ρ_{min} has the smallest upturn. In PLD608 the upturn increases with magnetic field whereas as ρ_{min} decreases. Finally, a comparison of the change in the upturn at 0T and 5T in the 'V' and the 'W' structures with the straight nanowires clearly indicates a larger decrease in the zigzag devices.

In Table 2 we determine some of the basic parameters of the electron-electron interactions for the different devices. First we compute the thermal lengths L_t (at 10K) and find them to be of order ~ 6-10 nm. While devices from PLD 608 and 664 should therefore be considered three-dimensional for electron-electron interactions because their thicknesses are sufficiently large, PLD 683, falls at the border between the two.

TABLE II. Key characteristics related to electron-electron interactions for the different devices. The value of $\breve{F}_{\sigma}^{x}$ where x = 2D or 3D is given at 5 T (4T for PLD608 dev 8).

Dev ref	t nm	Shape	D cm^2-sec^{-1}	L_t nm	*Dim*	$\breve{F}_{\sigma}^{x}$	Std dev
PLD664 dev 16	27.0 ± 0.4	V	1.13	10	3	0.865	0.008
PLD664 dev 30	27.0 ± 0.4	V	0.98	8.7	3	0.871	0.004
PLD608 dev 8	20.8 ± 0.4	NW	0.92	8.3	3	0.865	0.018
PLD608 dev 9	20.8 ± 0.4	NW	1.03	9.7	3	0.889	0.007
PLD683 dev17	9.6 ± 0.2	NW	0.44	5.1	2 3	0.746 0.876	0.008 0.001
PLD683 dev6	9.6 ± 0.2	NW	0.27	5.7	2 3	0.394 0.861	0.003 0.002
PLD683 dev22	9.6 ± 0.2	W	0.54	6.4	2 3	-0.645 0.812	- 0.01

Figure 3 shows sample fits to the 2D and 3D form of the electron-electron interactions at 5 T. These fits are done by transforming the resistivity (2D for devices from PLD 683 and 3D for devices from the other films) into conductivity and taking the appropriate functional dependence of the temperature. Table 2 also shows the fitting parameter $\breve{F}_{\sigma}^{x}$, where x = 2D or 3D, obtained for each of the devices We found that the devices from PLD 683 could be suitably fit using both Eq (6) and Eq (3), but that the values obtained for the three-dimensional fit are more consistent with those expected theoretically.

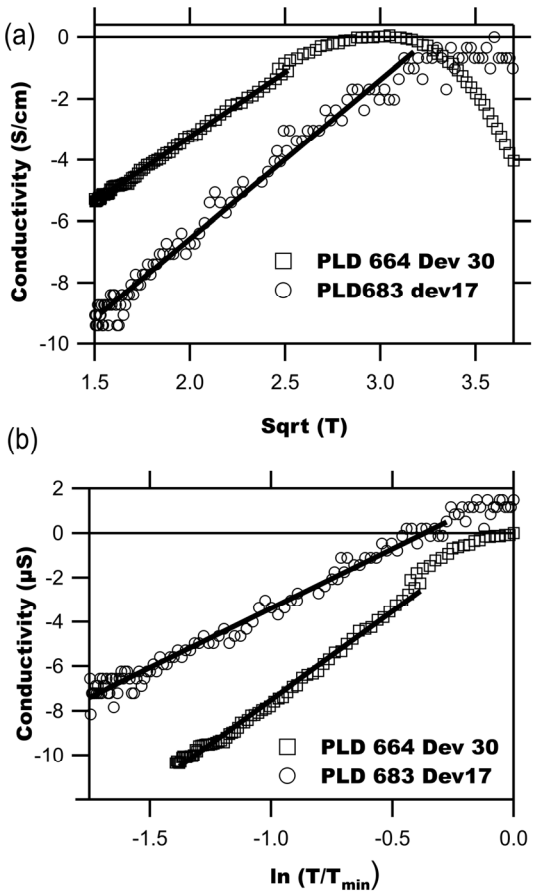

FIG.3. Fits of device PLD 664, Dev 30 from 2.2K to 6.3 K in a 5 T perpendicular field and PLD 683, Dev 17 from 9.5 K to 2.2 K in a 6 T perpendicular field to (a) the 3D EE interactions (Eq 3) and (b) 2D EE interactions (Eq 6). Note that the different units in the graphs correspond to three-dimensonal (a) and two-dimensional (b) conductivities. In (a) the fits to PLD 664 Dev 30 yield $\check{F}_{\sigma}^{3D} = 0.87$, and for PLD683, Dev 17 $\check{F}_{\sigma}^{3D} = 0.876$. In (b) the fits to PLD 664 Dev 30 result in $\check{F}_{\sigma}^{2D} = 0.916$, PLD683, Dev 17 $\check{F}_{\sigma}^{2D} = 0.746$.

B. Discussion

1. Electron-electron interactions explain the majority of the resistivity upturn

The basic result observed in Table II is that the data is consistent with three dimensional electron-electron interactions being the dominant cause of the resistivity upturn in all of the devices. Even though the thinnest films have a much larger upturn, suggesting the presence of another physical effect such as weak localization, this can also be interpreted in the context of EEI as a result of the larger ρ_{min}. To see this, we combine the equations (1), (3) and the definition of the diffusion coefficient to obtain the functional form of the fitting constant K:

$$K = K' e \rho_0^{2.5} \sqrt{N(E)} \tag{8}$$

where K' includes the prefactors and the screening constant in eq (3), found experimentally to be mostly constant across the different devices and fields. Thus changes in ρ_{min}, such as those observed with thickness, nano-patterning and magnetic field should naturally impact Δρ. Specifically, the *increase* in ρ_{min} with thickness correlates with the *increase* in Δρ and the *decrease* in ρ_{min} with magnetic field correlates with the *decrease* in Δρ.

To understand the changes with magnetic field, Fig. 4 shows $\check{F}_\sigma^x$ as function of magnetic field for the different devices. We note that the values obtained in two-dimensions are far from the expected values. In three dimensions, only PLD 683 Dev 22 significantly varies from the 0 T value. To understand the change with field, we reconsider equation (1). We note that with $\check{F}_\sigma^{3D} = 0.87$ the Hartree and Exchange terms are very similar so that changes in $\check{F}_\sigma^{3D}$ have a very small impact on the dependence, which is instead dominated by the $\sqrt{\frac{k_B T}{2\hbar D}}$ dependence. These observations suggests a reinterpretation of some results suggesting weak

localization at relatively high fields[35], but not those observed at very low fields[28].

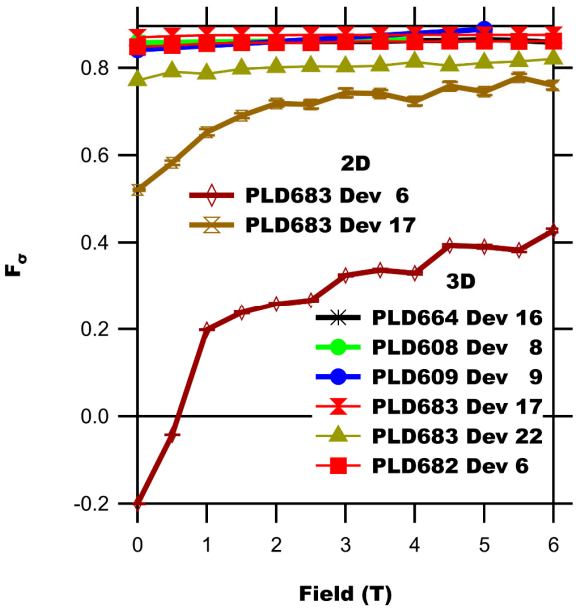

FIG.3. Plot of the electron-electron interaction constant $\breve{F}_\sigma^x$ as a function of magnetic field for the different devices.

Another physical effect that can occur at these temperatures and that resembles the ln(T) dependence of weak localization and two-dimensional electron-electron interactions is the Kondo effect. Here the resistivity upturn is due to an interaction between localized magnetic impurities and conduction electrons[36]. A wide variety of materials have been shown to exhibit the Kondo effect including dilute magnetic alloys[37], magnetic semiconductors[38], quantum dots[39] and most recently even non-magnetic materials without magnetic impurities[40]. In the devices considered here, however it seems unlikely that the Kondo effect could play a role because LSMO does not *a priori* contain localized magnetic impurities. One might consider that defects induced from the nanofabrication could interfere with the spin polarized conduction electrons, however this

does not appear to be likely either because film thickness is known to decrease the effectiveness of the Kondo effect[41] and this is where the resistivity upturn is seen to be the largest.

Some previous reports of resistivity upturn have been attributed to tunneling between nanoscale magnetic domains[18-20]. The fabrication process involved here, using electron beam lithography and ion beam etching, may damage the underlying crystallinity of the LSMO film and/or result in non-uniformities. Such effects could promote the formation of nanoscale magnetic domains, which can result in additional disorder and or change the resistivity. The most important evidence that the transport is not dominated by non-crystallinities is that all devices were ohmic down to the lowest temperatures, as shown in Figure S2. Nevertheless, the variations observed in ρ_{min} hint that nanoscale magnetic domains and disorder do arise in nano-patterned samples, as we now explore.

2. Impact of nano-patterning on the low temperature magneto-transport

We first consider the impact of the difference between the effective transport thickness and the physical device thickness, a distinction that is more likely to be more important for thinner films. Specifically, an interfacial layer of ~ 3 nm between LSMO and STO (100) arises and is insulating so that its contribution to the transport is minimal. For the 9.6 nm thin film, ρ_{min} would therefore be significantly larger, however, the effective ρ_{min}, which accounts for a true transport thickness, would be 70% smaller and could not alone account for the larger ρ_{min}. It is therefore more likely that the increased resistivities in thinner films are due to enhanced scattering at the surface[42].

Similarly, we expect enhanced surface roughness scattering to increase ρ_{min} in the smaller width devices. It is likely that the increase in ρ_{min} observed in the two devices in PLD664 corresponds to this mechanism. In Table 1, however, we observed instead that ρ_{min} *decreases* with nano-patterned width in the devices in PLD608 and PLD683. We believe that in these larger width devices scattering at magnetic domains accounts for these differences in ρ_{min}. Magnetic domains may play an important role in device widths down to 350-400 nm, which are approximately the size of a single out of plane domain[43].

Changes in the resistivity upturn will be dominated by the constant K given in eq (8), which has a very large ρ_{min} dependence and a smaller dependence on N(E). Thus the changes at 0 T of $\Delta\rho$ closely resemble the changes in ρ_{min}, for instance the larger ρ_{min} in the wider devices of PLD608 exhibits a larger $\Delta\rho$. This is not the case, however in PLD683. Specifically, in dev 17 ρ_{min} is larger than in dev 6 but exhibits a smaller upturn. This 'lack' of a larger $\Delta\rho$ is likely due to important magnetic domains because ρ_{min} decreases significantly more in field than dev 6. These non-uniformities are found to affect both the high T, through the fitting parameter b, and the low T. We thus see that even with ohmic behavior, the magnetic domains can play an important role in nano-patterned devices.

The impact of changes in the high temperature transport are most notable in varations in T_{min}. T_{min} occurs at the intersection of eqs. (1) and (2) and is found to be:

$$T_{min} = \rho_0^{1.25}\sqrt{\frac{K' e\sqrt{N(E)}}{b}} \qquad (9)$$

In Table S1 we observe the change in ρ_{min} with width correlates with a higher T_{min} in PLD 664 and PLD 608, but not in PLD683. From eq (9) through we see that decreases in the constant b in the devices in PLD683 compensate for the decreases in ρ_{min}. As a result,

values for T_{min} that do not vary as much as expected given the changes in ρ_{min}. Interpretations of changes in T_{min} can thus be complex involving several different physical phenomena.

The changes in $\Delta\rho$, ρ_{min}, and T_{min} with magnetic field vary quite a bit among the samples. For the 'V' and 'W' nanowires in PLD664 and PLD683, the devices exhibit the largest changes in ρ_{min} with magnetic field and the correspondingly largest decreases in $\Delta\rho$. Such changes are attributed to the domains that arise and impede transport in the different arms of these zigzag devices. By comparison the changes in ρ_{min} of the PLD608 devices with field are very small and $\Delta\rho$ increases. We attribute this to an increase in *N(E)* with magnetic field, as one might expect from band structure calcaluations[34]. This effect can also explain the observed increases in T_{min}.

Finally, the devices in PLD664 are patterned in a different crystallographic direction than PLD608 and one might therefore wonder if this might change the interaction parameter. Using[34] $k_{\parallel} = 0.4\ \pi/\mathrm{a}$, we find that and $\check{F}_{\sigma}^{x3D} = 0.89$, which for the devices observed here is so close to the value obtained for $k_f = 0.49\ \pi/\mathrm{a}$, that we would not be able to distinguish them in our experiments. It should be noted that the similarity in the Hartree and Exchange terms in equation (1) supports this conclusion.

V. SUMMARY AND CONCLUSIONS

We have investigated the magneto-transport through epitaxial nano-patterned LSMO thin films with thicknesses smaller than 30 nm at low temperatures. We observe a resistivity minimum in all of these devices and find that electron-electron interactions can explain the data with a very good correspondence between the fitted and theoretical value of

$\check{F}_{\sigma}^{3D} = 0.87$. We find that this effect can also explain small decreases in the resistivity minimum at large magnetic fields. We find that narrower width devices down to 350 nm exhibit smaller ρ_{min}, which are attributed to a reduction in magnetic domain scattering. We also find that 'V' and 'W' shape wires exhibit a greater decrease in the resistivity upturn with magnetic field, which is attributed to the alignment of the domains as the field increases.

ACKNOWLEDGMENTS

This research was partially funded by Triangle de la Physique(RTRA) contract MolSpinOx # 2008-022T.

[1] P.A. Lee and T.V. Ramakrishnan, Rev. Mod. Phys. **57**, 287 (1985).
[2] G. Bergmann, Phys. Rep. **107**, 1 (1984).
[3] J.J. Lin and J.P. Bird, J. Phys. Condens. Matter **14**, R501 (2002).
[4] V.K. Dugaev, P. Bruno, and J. Barnaś, Phys. Rev. B **64**, 144423 (2001).
[5] T. Ono, Y. Ooka, S. Kasai, H. Miyajima, K. Mibu, and T. Shinjo, J. Magn. Magn. Mater. (2001).
[6] M. Brands, A. Carl, O. Posth, and G. Dumpich, Phys. Rev. B **72**, 085457 (2005).
[7] M. Brands, C. Hassel, A. Carl, and G. Dumpich, Phys. Rev. B **74**, 033406 (2006).
[8] C. Hassel, F.M. Römer, G. Dumpich, and J. Lindner, Phys. Rev. B **79**, 092417 (2009).
[9] D. Neumaier, K. Wagner, S. Geißler, U. Wurstbauer, J. Sadowski, W. Wegscheider, and D. Weiss, Phys. Rev. Lett. **99**, 116803 (2007).
[10] D. Neumaier, A. Vogl, J. Eroms, and D. Weiss, Phys. Rev. B **78**, 174424 (2008).
[11] S. Sil, P. Entel, G. Dumpich, and M. Brands, Phys. Rev. B **72**, 174401 (2005).
[12] M. Aprili, J. Lesueur, L. Dumoulin, and P. Nédellec, Solid State Commun. **102**, 41 (1997).
[13] R. Misra, A.F. Hebard, K.A. Muttalib, and P. Wölfle, Phys. Rev. B **79**, 140408 (2009).
[14] V.K. Dugaev, P. Bruno, and J. Barnaś, Phys. Rev. Lett. **101**, 129701 (2008).
[15] P. Mitra, R. Misra, A.F. Hebard, K.A. Muttalib, and P. Wölfle, Phys. Rev. Lett. **99**, 046804 (2007).
[16] N. Kurzweil, E. Kogan, and A. Frydman, Phys. Rev. B **82**, 235104 (2010).
[17] Y. Wu, Y. Matsushita, and Y. Suzuki, Phys. Rev. B **64**, 220404 (2001).
[18] E. Rozenberg, M. Auslender, I. Felner, and G. Gorodetsky, J. Appl. Phys. **88** 2578 (2000).
[19] S. Mukhopadhyay and I. Das, J. Phys. Condens. Matter **21**, 186004 (2009).
[20] M. Auslender, A.E. Kar'kin, E. Rozenberg, and G. Gorodetsky, J. Appl. Phys. **88** 6639 (2001).
[21] P. Chen, D.Y. Xing, and Y.W. Du, Phys. Rev. B **64**, 104402 (2001).

[22] D. Kumar, J. Sankar, J. Narayan, R.K. Singh, and A.K. Majumdar, Phys. Rev. B **65**, 094407 (2002).
[23] G. Herranz, F. Sánchez, J. Fontcuberta, V. Laukhin, J. Galibert, M.V. García-Cuenca, C. Ferrater, and M. Varela, Phys. Rev. B **72**, 014457 (2005).
[24] J. Zhang, Y. Xu, L. Yu, S. Cao, and Y. Zhao, Phys. B Condens. Matter **403**, 1471 (2008).
[25] R.R. Jia, J.C. Zhang, R.K. Zheng, D.M. Deng, H.-U. Habermeier, H.L.W. Chan, H.S. Luo, and S.X. Cao, Phys. Rev. B **82**, 104418 (2010).
[26] M. Ziese, Phys. Rev. B **68**, 132411 (2003).
[27] L. Maritato, C. Adamo, C. Barone, G.M.D. Luca, A. Galdi, P. Orgiani, and A.Y. Petrov, Phys. Rev. B **73**, 094456 (2006).
[28] W. Niu, M. Gao, X. Wang, F. Song, J. Du, X. Wang, Y. Xu, and R. Zhang, Sci. Rep. **6**, 26081 (2016).
[29] S.-P. Chiu, M. Yamanouchi, T. Oyamada, H. Ohta, and J.-J. Lin, Phys. Rev. B **96**, 085143 (2017).
[30] L.E. Calvet, G. Agnus, Y. Vaheb, Y.C. Lau, V. Pillard, and P. Lecoeur, Thin Solid Films **520**, 4600 (2012).
[31] F. Gaucher, A. Pautrat, S. Autier-Laurent, C. David, L.E. Calvet, P. Lecoeur, and A.-M. Haghiri-Gosnet, Microelectron. Eng. **86**, 820 (2009).
[32] X. Wang and X.-G. Zhang, Phys. Rev. Lett. **82**, 4276 (1999).
[33] B.F. Woodfield, M.L. Wilson, and J.M. Byers, Phys. Rev. Lett. **78**, 3201 (1997).
[34] J. Krempaský, V.N. Strocov, L. Patthey, P.R. Willmott, R. Herger, M. Falub, P. Blaha, M. Hoesch, V. Petrov, M.C. Richter, O. Heckmann, and K. Hricovini, Phys. Rev. B **77**, 165120 (2008).
[35] L. Maritato, C. Adamo, C. Barone, G.M.D. Luca, A. Galdi, P. Orgiani, and A.Y. Petrov, Phys. Rev. B **73**, 094456 (2006).
[36] J. Kondo, Prog. Theor. Phys. **32**, 37 (1964).
[37] A.F.G. Wyatt, Phys. Rev. Lett. **13**, 401 (1964).
[38] H.T. He, C.L. Yang, W.K. Ge, J.N. Wang, X. Dai, and Y.Q. Wang, Appl. Phys. Lett. **87**, 162506 (2005).
[39] D. Goldhaber-Gordon, H. Shtrikman, D. Mahalu, D. Abusch-Magder, U. Meirav, and M.A. Kastner, Nature **391**, 156 (1998).
[40] K.R. Sapkota, F.S. Maloney, and W. Wang, Phys. Rev. B **97**, 144425 (2018).
[41] G. Chen and N. Giordano, Phys. Rev. Lett. **66**, 209 (1991).
[42] S. Mukhopadhyay and I. Das, J. Phys. Condens. Matter **21**, 186004 (2009).
[43] E.P. Houwman, G. Maris, G.M.D. Luca, G.M.D. Luca, N. Niemann, A.J.H.M. Rijnders, D.H.A. Blank, and S. Speller, Phys. Rev. B Condens. Matter Mater. Phys. **77**, 174412 (2008).
[44] See supplementary material at https://doi.org/10.1116/1.5085669 for for SEMs, ohmic I-V behavior, fitting parameters and the resistivity upturn at zero and finite magnetic field for all devices.

Dev ref	t nm	l µm	w µm	Shape	ρ_{min} mΩ-cm	T_{min} (0T) K	upturn (0T) %	T_{min} (5T) K	upturn (5T) %
PLD664 dev 16	27 ± 0.4	2	0.13	V	0.231	10.3	0.3	10.4	0.21
PLD664 dev 30	27 ± 0.4	2	0.11	V	0.265	11.7	0.29	11.7	0.21
PLD608 dev 8	20.8 ± 0.4	30	0.8	NW	0.277	11.6	0.39	11.93	0.43
PLD608 dev 9	20.8 ± 0.4	30	0.35	NW	0.254	10.7	0.50	12.5	0.61
PLD683 dev17	9.6 ± 0.2	1.67	0.4	NW	0.955	14.3	1.7	12.2	1.1
PLD683 dev6	9.6 ± 0.2	1.8	0.138	NW	0.593	14.5	1.9	15.3	1.05
PLD683 dev22	9.6 ± 0.2	$\sum_i \frac{l_i}{w_i} = 42.3$		W	0.479	13.94	4	14.57	2.2

TABLE I. Key characteristics of the different devices. The shape column indicates the geometry of the device. 'V' and 'W' indicate a V and W type nano-patterning, as shown in the supplementary material, in which the transport is along the (100) direction. 'NW' indicates a straight nanowire with the transport along the (110) easy axis. The 'W' nanowires in PLD683 dev 22 had widths of 119 nm, comparable to the NW in PLD683 dev 6. Note that the magnetic field data in PLD608 dev 8 was done at 4 T.

Dev ref	t nm	Shape	D cm^2-sec^{-1}	L_t nm	*Dim*	$\breve{F}_\sigma^x$	Std dev
PLD664 dev 16	27.0 ± 0.4	V	1.13	10	3	0.865	0.008
PLD664 dev 30	27.0 ± 0.4	V	0.98	8.7	3	0.871	0.004
PLD608 dev 8	20.8 ± 0.4	NW	0.92	8.3	3	0.865	0.018
PLD608 dev 9	20.8 ± 0.4	NW	1.03	9.7	3	0.889	0.007
PLD683 dev17	9.6 ± 0.2	NW	0.44	5.1	2 3	0.746 0.876	0.008 0.001
PLD683 dev6	9.6 ± 0.2	NW	0.27	5.7	2 3	0.394 0.861	0.003 0.002
PLD683 dev22	9.6 ± 0.2	W	0.54	6.4	2 3	-0.645 0.812	- 0.01

TABLE II. Key characteristics related to electron-electron interactions for the different devices. The value of $\breve{F}_\sigma^x$ where x = 2D or 3D is given at 5 T (4T for PLD608 dev 8.)

Figure Captions

FIG. 1. (a) Resistivity versus temperature at 0 T and 4 T for a) PLD 608 dev 8 and b) PLD 683, dev 17. The curves are normalized so that the minimum of the 4 T curve overlaps that of the 0 T curve. The insets show SEMs of the devices. SEMs and curves for all devices are shown in Fig. S1 and Fig. S3 respectively.

Fig. 2. Resistivity upturn at 0T and 5T for PLD 683 Device 6 showing the data (markers) and fits to Eqs (1) and (2) above where the intersection was used to determine % upturn, ρ_{min}, T_{min} for Table 1.

FIG.3. Fits of device PLD 664, Dev 30 from 2.2K to 6.3 K in a 5 T perpendicular field and PLD 683, Dev 17 from 9.5 K to 2.2 K in a 6 T perpendicular field to (a) the 3D EE interactions (Eq 3) and (b) 2D EE interactions (Eq 6). Note that the different units in the graphs correspond to three-dimensonal (a) and two-dimensional (b) conductivities. In (a) the fits to PLD 664 Dev 30 yield $\breve{F}_{\sigma}^{3D} = 0.87$, and for PLD683, Dev 17 $\breve{F}_{\sigma}^{3D} = 0.876$. In (b) the fits to PLD 664 Dev 30 result in $\breve{F}_{\sigma}^{2D} = 0.916$, PLD683, Dev 17 $\breve{F}_{\sigma}^{2D} = 0.746$.

FIG.4. Plot of the electron-electron interaction constant $\breve{F}_{\sigma}^{x}$ as a function of magnetic field for the different devices.